COMMUNICATION

High Polymer/Fullerene Ratio Realized in Efficient Polymer Solar Cells by Tailoring of the Polymer Side-Chains

*Jianyu Yuan, Huilong Dong, Ming Li, Xiaodong Huang, Jun Zhong, Youyong Li, and Wanli Ma**

Solution-processed polymer solar cells (PSCs) can be fabricated on plastic substrates, offering advantages such as light weight, mechanical flexibility, and semi-transparency.[1] Bulk heterojunction (BHJ) PSCs that contain a blend film of a conjugated polymer and fullerene derivative, such as phenyl-C61-butyric acid methyl ester ($PC_{61}BM$), as the active layer has been studied most extensively.[2] By optimizing the molecular structure and device architecture, power conversion efficiency (PCE) values that approach 10% have been achieved recently.[3] Generally, the optimal blend ratio of polymer/fullerene (D/A) in PSCs is larger than 1:1 by weight, with some close to 1:4.[4] However, a high polymer/fullerene ratio is desired since the inherent tendency of fullerene to aggregate under elevated temperatures has been considered a key factor for deteriorated morphology and consequently reduced lifetime of PSCs.[5] Furthermore, conventional $PC_{61}BM$ demonstrates weak absorbance in the visible region, leading to inefficient photon harvesting. The use of thick films can improve absorbance but often causes increased recombination and a degraded fill factor (FF) because of the limited carrier mobilities in organic materials. Therefore, high polymer/fullerene ratios allow high absorbance for relatively thin films to avoid such problems and may improve device thermal stability. From the point view of industrial coating processes, low fullerene loading can also increase the photochemical and mechanical film robustness and allow better control of the solution viscosity. Search strategies to reduce the use of fullerene in PSCs are thus important, but this has rarely been studied. The tailoring of the polymer side-chains may be an effective method to realize a high polymer/fullerene ratio, according to McGehee et al.,[6] in which the microscopic mechanism that determines the optimum polymer/fullerene blend ratios was discussed. The authors claimed that if the side-chain spacing of polymers has sufficient free volume allowing for fullerene intercalation, highly ordered bimolecular crystals are likely to form, which leads to a high level of fullerene loading. In contrast, dense polymer side-chains can prevent fullerene intercalation and result in a low optimal fullerene ratio. In their following work, the existence of bimolecular crystals was confirmed by the use of X-ray diffraction, molecular simulations, and spectroscopy.[7] Note that the polymers studied in their original work were based on different backbones, which introduced extra complexity and might weaken their conclusions. Additionally, no following work on molecular design has been performed to strengthen their theory. Therefore, inspired by their work, we used alternating donor-acceptor (D-A) conjugated polymers based on the same backbone, with benzo[1,2-b:4,5-b′]dithiophene (BDT) as the donor monomer and N-alkyl-thieno[3,4-c]pyrrole-4,6-dione (TPD) as the acceptor monomer for investigation. This BDT-TPD backbone has been well studied and polymers based on it have demonstrated both good PCEs of 4–7% and large open-circuit voltages (V_{oc}) of 0.8–1.0 V.[8] This popular backbone was intentionally chosen for the side-chain modification to demonstrate that this strategy may become a simple and universal way to reduce the use of PCBM for existing efficient polymers. The free volume between side-chains can be adjusted by substituting alkyl chains with alkylthienyl or alkylphenyl ones, which are less flexible and more bulky than alkyl chains. In addition, the introduction of conjugated side chains to BDT-based D-A copolymers can result in more planar configuration and fine-tuned energy levels, leading to improved device performance in both PSCs and organic field effect transistors (OFETs).[9] It is worth noting that we also appended alkyl aromatic side chains to the acceptor comonomer to further adjust the side-chain spacing, while the density of side-chains was altered by incorporating conjugated π-bridge to the polymer backbone. In this work, aiming to reduce the use of fullerene, we performed systematical side-chain modification on BDT-TPD based polymers (**Scheme 1**). A novel D-A copolymer PTP8 with alkyl aromatic side-chains on both donor and acceptor comonomer was firstly synthesized. A high V_{oc} of 0.96 V and PCE of 6.18% were achieved for PTP8:$PC_{71}BM$ based BHJ PSCs at a low blend ratio of 1:0.8. Furthermore, the device performance showed a weak dependence on the PCBM concentration, demonstrating a relatively high PCE even at an extremely low blend ratio of 1:0.3. Interestingly, with lower PCBM concentrations, less solvent additive was required to achieve the optimal morphologies, suggesting a more environment-friendly fabrication process. As a result, the introduction of alkyl aromatic side-chains to both D/A monomers may become a general approach adopted in molecular design to effectively adjust the interaction between fullerene and polymers, leading to reduced use of PCBM and additives. Recently, Hou et al. reported a novel polymer that demonstrated a high PCE of 6.88% in PSCs with relatively low PCBM loadings.[10] The high D/A ratio was attributed to

J. Yuan, H. Dong, M. Li, X. Huang, J. Zhong, Y. Li, Prof. W. Ma
Institute of Functional Nano & Soft Materials (FUNSOM)
Jiangsu Key Laboratory for Carbon-Based Functional Materials & Devices
Soochow University
Collaborative Innovation Center of Suzhou Nano Science and Technology
Soochow University
199 Ren-Ai Road, Suzhou Industrial Park, Suzhou, Jiangsu 215123, P. R. China
E-mail: wlma@suda.edu.cn

DOI: 10.1002/adma.201305577

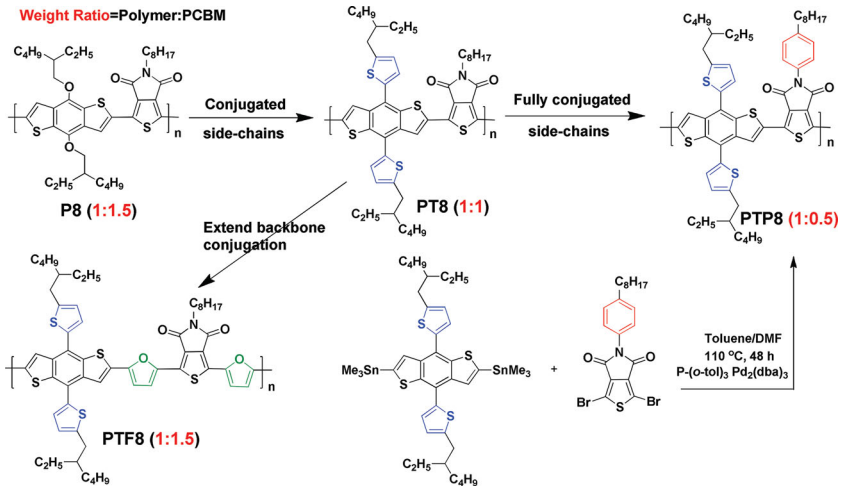

Scheme 1. The synthetic route of PTP8 and molecular structures of a series of BDT-TPD based D-A polymers. The red numbers refer to the polymer's optimal blend ratios.

the compact interchain packing between polymer backbones. However, it was not explained in detail how the small lamellar spacing led to the reduced use of PCBM. We realized that in such a complex blend system, the interaction between polymers and PCBM may affect the D/A ratio in both mesoscopic and microscopic scale. Therefore we performed elaborate study on the blend film morphology and carried out theoretical simulation at the molecular level to investigate the possible factors influencing D/A ratios.

Polymer PTP8 was synthesized as illustrated in Scheme 1. Alkylphenyl side-chains were appended to TPD block following a reported method,[11] The synthesis of other polymers is described in the experimental section. Systematical characterizations of the BDT-TPD based polymers were carried out, focusing on investigating the effect of alkyl aromatic side-chains on material properties. Thermal stability of polymer P8, PT8 and PTP8 was investigated by thermo gravimetric analysis (TGA) at a temperature ramp rate of 10 °C/min under N_2. As shown in Figure S2a, the decomposition temperature (T_d) of P8, PT8 and PTP8 is 352 °C, 423 °C and 456 °C, respectively. The largely improved thermal stability of PT8 and PTP8 over P8 can be attributed to the π-conjugated side-chains on BDT donor block.[9] The further increased T_d of PTP8 is likely resulting from the alkylphenyl chain introduced to the TPD acceptor monomer, suggesting that alkyl aromatic side-chains on either donor or acceptor block can effectively improve polymer thermal stability. The optical properties of the PT8 and PTP8 were investigated by UV-vis-NIR absorption spectroscopy in solution and as-cast thin films, as shown in Figure S2b. Compared to PT8, PTP8 shows a broader absorption spectrum both in solution and film. A ~40 nm red-shift can also be observed in the absorption spectrum of PTP8 film, indicating the enhanced polymer packing induced by the alkylphenyl group on the acceptor block. The corresponding optical band-gap (E_g^{opt}) calculated from the absorption edge of polymer films is 1.85 eV and 1.78 eV for PT8 and PTP8, respectively. The polymer energy levels were theoretically calculated by performing density functional theory (DFT) studies on Gaussian 09. We discovered that the decreased band-gap was mostly arising from the shift of the polymer lowest unoccupied molecular orbital (LUMO) energy levels (Figure S3). Thus the introduction of alkylphenyl chains on the acceptor block can lower the polymer LUMO by effectively extending the electron orbit distribution, while previous reports indicated that the alkylthienyl chains on the donor block mainly influenced the polymer highest occupied molecular orbital (HOMO) level.[9e,f] The polymer energy levels were also measured by cyclic voltammetry (CV, Figure S4). The HOMO and LUMO energy levels, calculated from onset of the oxidation and reduction peaks in cyclic voltammograms, are −5.59 eV, −5.61 eV and −3.62 eV, −3.56 eV for PTP8 and PT8[10f] respectively, which is consistent with the DFT theoretical calculation.

PSCs were fabricated using a conventional architecture of ITO/PEDOT-PSS(40 nm)/Polymer:PCBM/LiF(0.6 nm)/Al(100 nm), as shown in **Figure 1**a. The device optimization includes fine adjustment of solvents (Table S1), film thickness, additives concentration, blend ratio (Table S2) and fullerene types (Tables S3). Throughout the experiment, a fixed polymer concentration of 8 mg/mL was adopted. 1,8-diiodooctane (DIO) was used as solvent additive to improve film morphology, which has been extensively studied in previous work in PSCs.[12] The *J*–*V* characteristics of the optimized devices based on PTP8:$PC_{71}BM$ with different blend ratios are shown in Figure 1b with the detailed parameters listed in **Table 1**. All the devices exhibit high V_{oc} around 1.00 V. And relatively high PCEs of 5.45%, 6.18%, 5.77%, 5.98%, and 4.04% are achieved at the weight ratio of 1:1, 1:0.8, 1:0.6, 1:0.5 and 1:0.3, respectively. It is worth noting that the optimal DIO concentrations are reduced with lower $PC_{71}BM$ loadings, as shown in the insert of Figure 1b and Figure S5. Similar trend was observed in small molecule solar cells at low PCBM loadings,[13] while this observation was firstly reported by us in polymer solar cells. To evaluate the photo-response of PTP8 based devices and calibrate the J_{sc} data, external quantum efficiencies (EQE) of optimized devices with different blend ratios were measured and shown in Figure 1c. The devices show relatively high photo-conversion efficiency over the whole wavelength range (370–680 nm), with monochromatic EQE values around 50–60%. The J_{sc} calculated by integrating the EQE curve with an AM1.5G reference spectrum is within ~3% error compared to the corresponding J_{sc} obtained from the *J*–*V* curves. From the device performance, we note that a high PCE approaching 6% is achieved at a blend ratio of 1:0.5, which is among the highest efficiencies for PSCs with such a low PCBM concentration. And the PCE remains fairly stable with the bend ratio varying from 1:0.5 to 1:0.8, while the PCE of P8, PT8 based devices drastically decreases once the PCBM loading is lower than the optimal concentration (Figure 1d). As shown in Table S4, the optimal blend ratio for P8, PT8 and PTP8 is 1:1.5, 1:1 and 1:0.8 respectively. According to the work of McGehee et al., the blend ratios and polymer side-chain structures can be closely correlated in molecular level. With flexible alkyl side-chains on both

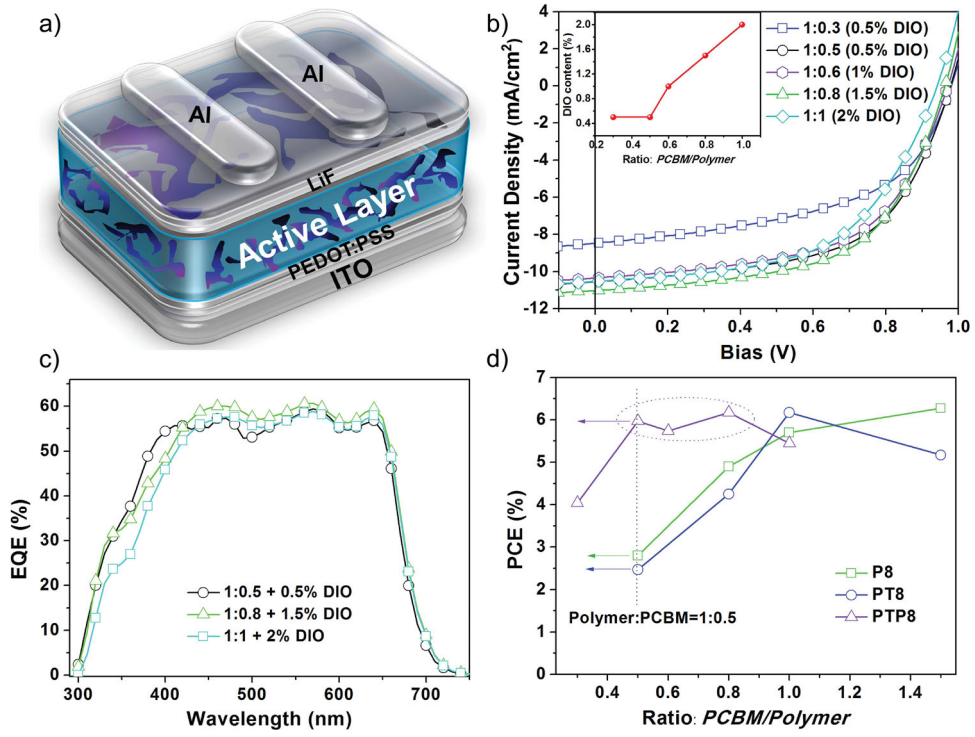

Figure 1. a) Device structure of the investigated polymer solar cells b) *J–V* curves of optimized PSCs based on PTP8:$PC_{71}BM$ with different blend ratios (the insert shows DIO concentrations VS blend ratios) c) EQE of optimized PSCs with different blend ratios d) effect of polymer/PCBM weight ratios on the performance of device based on P8, PT8 and PTP8. The PCE of PTP8 based PSCs show weak dependence on the blend ratios.

D/A comonomers, P8 has the largest free volume. Fullerene intercalation can be easily realized, thus a large amount of fullerene (1:1.5) is required to fill in the side-chain spacing and then form the pure electron transporting phase. In contrast, with bulky aromatic chains on both D/A blocks, intercalation is prevented and a smaller amount of fullerene (1:0.8) is sufficient to form continuous fullerene network. PT8 has one alkyl and one alkyl aromatic side-chain, resulting in a moderate blend ratio of 1:1 between that of P8 and PTP8. Interestingly, if we introduce a conjugated furan π-bridge to the PT8 backbone and obtain PTF8, the optimal blend ratio changes back from 1:1 to 1:1.5 as a result of the increased side-chain spacing. It is worth noting that in our previous work, the optimal blend ratio for PSCs based on poly(3-hexylthiophene) (P3HT) is also 1:0.8,[14] similar to that of PTP8. Both polymers have large side-chain densities, indicating that the interaction between fullerene and side-chains, rather than the different backbone structures, has more impact on the optimal blend ratio. To confirm the correlation between polymer side-chains and the device optimal blend ratios, simplified theoretical simulations of molecular dynamics were performed. We are well aware that the simulation focuses only on microscopic D/A interaction without considering mesoscopic factors that might also affect the blend ratio. Thus we will address those issues during the morphology investigation. According to the simulation results (Figure S6), the interaction between fullerenes and aromatic side-chains is stronger than that between alkyl ones. Thus shallower fullerene intercalation is expected for polymers with aromatic side-chains, while deeper fullerene intercalation is allowed for polymers with flexible alkyl side-chains. In short, the theoretical simulation demonstrates that the side-chain structure is very likely one of the key factors determining the blend ratios in PSCs. It is worthwhile noting that this conclusion actually coincides well with the observation in Hou's work.[10] Although they didn't mention fullerene intercalation, they did observe very small lamellar spacing which, however, clearly suggested that fullerene intercalation was unlikely to occur due to the close packing.

Table 1. Optimized Devices performance of PTP8 with different $PC_{71}BM$ weight ratios.

Ratio w/w	V_{oc} [V]	J_{sc} [mA/cm^2]	FF [%]	PCE [%]
1:1	0.93	10.50	55.7	5.44
1:0.8	0.96	11.00	58.5	6.18
1:0.6	0.97	10.32	57.6	5.77
1:0.5	0.98	10.51	58.1	5.98
1:0.3	1.00	8.42	48.0	4.04
1:0.1	0.76	1.45	28.5	0.32

The forming of continuous carrier paths is crucial to the charge mobility and device performance. To evaluate the charge transport at different blend ratios, the electron and hole mobility of PTP8/$PC_{71}BM$ blend film was measured by using space charge limited current (SCLC) technique. The results are shown in Figure S7, Figure S8 and Table S5. The calculated electron mobility is 8.52×10^{-6}, 2.34×10^{-5}, 2.85×10^{-5}, and 2.49×10^{-5} cm^{2}V^{-1}s^{-1} for the films with a blend ratio of

1:0.3, 1:0.5, 1:0.8, and 1:1, respectively, and the calculated hole mobility is 2.30×10^{-5}, 2.92×10^{-5}, 3.71×10^{-5}, and 3.42×10^{-5} $cm^2 V^{-1} s^{-1}$ for the film with a blend ratio of 1:0.3, 1:0.5, 1:0.8, and 1:1, respectively. The measured hole mobility of PTP8:PCBM is comparable to the value reported by McGehee and his coworkers.[8f] However, the FF of PTP8:PCBM device is relatively lower than theirs. We speculate that their different device processing conditions may directly impact the film morphology and hence device parameters. We observed that the electron mobility is almost the same for films with a blend ratio larger than 1:0.5, indicating the forming of continuous electron pathways above that ratio. With a lower blend ratio of 1:0.3, a significantly lower electron mobility is demonstrated, suggesting that the interconnected network of pure fullerene phases can no longer be developed with such low fullerene loading. As reported in the previous work, the interaction of fullerene and polymer may greatly change the hole mobility of the blend film.[15] We noted that the hole mobility is almost unchanged in our case with increased blend ratios, which indicate that the PCBM intercalation does not occur with all the blend ratios. We also measured the hole mobility of the pristine polymer films of P8, PT8 and PTP8 (Figure S9, Table S6), which shows that the side-chain modification does not evidently change the polymer hole mobility.

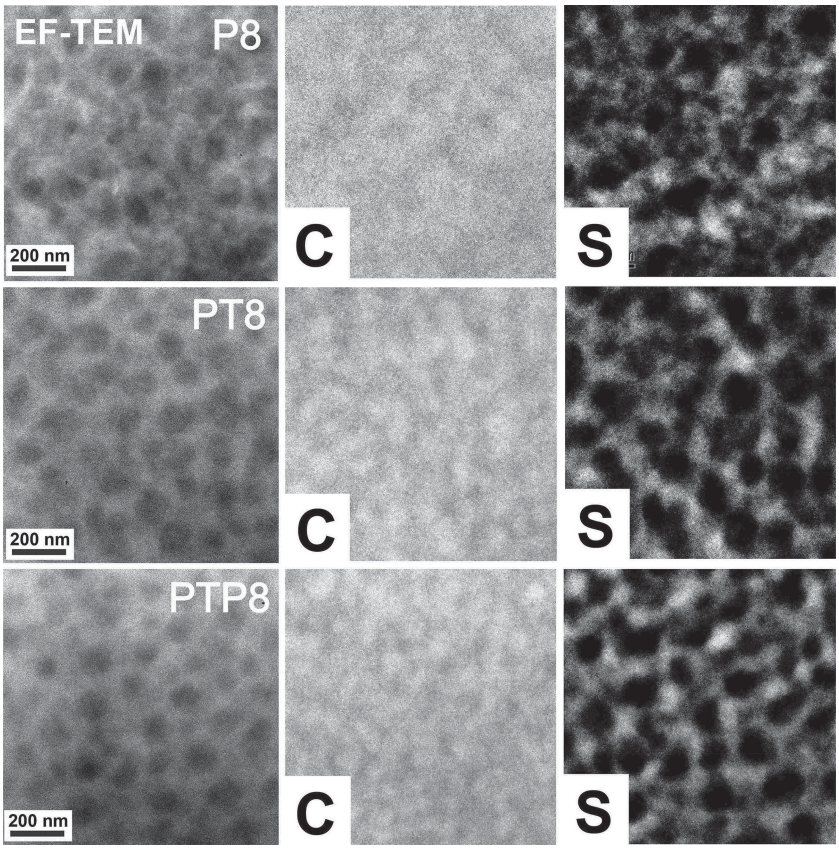

Figure 2. Bright-field and corresponding carbon edge and sulfur edge EELS maps of 1:0.5 wt ratio blend films for P8, PT8 and PTP8. The films were cast from pure chloroform to avoid the effect of additive on miscibility and morphology. The low fullerene ratio was used to prevent excessive PCBM aggregation. The scale is the same for all nine images.

In order to achieve high D/A ratio in a complex blend system, prevention of intercalation may not be sufficient. The blend morphology, which is largely determined by the polymer:fullerene and polymer:polymer interaction in mesoscopic level, may also have important impact on the D/A ratios. Additionally, by using minimum fullerene to develop continuous electron-transporting network requires desired morphologies as well. Thus thorough morphology investigations were carried out to gain comprehensive understanding of the mechanism for high D/A ratios by using tapping mode atomic force microscopy (AFM), scanning electron microscopy (SEM), transmission electron microscopy (TEM) and high-angle annular dark field scanning transmission electron microscopy (HAADF-STEM). The blend film morphology largely relies upon the polymer:fullerene miscibility, which has been reported to change drastically by minor side-chain modifications.[16] Therefore, the miscibility between fullerene and polymers with tailored side-chains should be compared and its effect on the film morphology and D/A ratios should be carefully investigated. Recently the polymer:fullerene miscibility has been measured by Treat et al. using dynamic secondary ion mass spectrometry and HAADF-STEM,[17a,b] by Collins et al. using near-edge X-ray absorption fine structure spectroscopy and grazing-incidence wide-angle X-ray scattering (GIWAXS),[17c–e] by Yin et al. using small-angle neutron scattering,[17f] by Kozub et al. using energy-filtered TEM (EFTEM) [17g] and by Jen et al. using surface energy measurement.[17h,18] EF-TEM was performed to investigate the possible miscibility and morphology change caused by side-chain modification, which allows for enhanced materials contrast and mapping of the local elemental composition.[17g] As shown in the bright-field images in **Figure 2**, the dark PCBM-rich domains in the blend films of PT8 and PTP8 have similar sizes and distributions, while the mixing in the blend film of P8 is slightly better. This observation is clearer and confirmed in the sulfur edge EELS (electron energy loss spectra) maps which show more contrast than the bright field image with the intensity of the elemental maps directly proportional to the polymer concentration within domains. Nonetheless, the contrast in carbon edge EELS map is decreased, possibly due to some amount of evenly mixed PCBM at molecular level. According to the report of Ade and his coworkers, the domain size and relative domain purity are overall correlated with molecular miscibility.[16] Since similar morphologies were observed for the blend films, we concluded that the miscibility of the three polymers is not significantly changed by the side-chain modification.

By using GIWAXS, we further investigated and compared the polymer:fullerene and polymer:polymer interactions for these three polymers. As shown in the scattering spectra of pristine PT8 (Figure S10a) and PTP8 (**Figure 3**a), the (010) peak

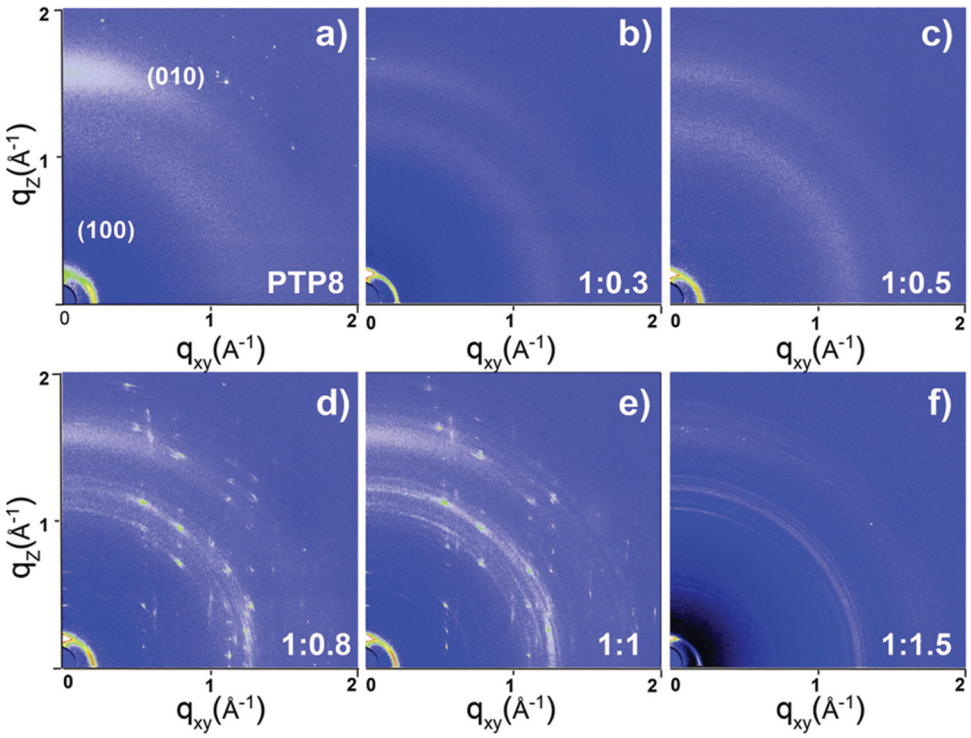

Figure 3. GIWAXS patterns of pristine PTP8 film cast from chloroform (a), PTP8:$PC_{71}BM$ blend films with different weight ratios cast from chloroform with optimized DIO concentrations (b-f). Note that the 2D spectra have not been corrected for the "missing wedge" of data along the out-of-plane direction.[19]

corresponding to π–π stacking is more pronounced in the out-of-plane direction, which suggests that majority of the polymer π–faces are parallel to the substrate. Note that the face-on orientation is adopted by all the three polymers P8,[9d] PT8 and PTP8, regardless of their different side-chain structures. As extracted from the out-of-plane GIXD files (**Figure 4**a), the lamella and π–π stacking distance is 21.36/3.69 Å and 22.92/3.56 Å for PT8 and PTP8 pristine films, respectively. The increased side-chain length of PTP8 over PT8 likely leads to its increased lamella distance, [20] which is, however, fixed with increased fullerene concentration, indicating that no intercalated phases are formed. The reduced π–π stacking distance of PTP8 compared to PT8 may benefit from the alkylphenyl side-chain on the TPD monomer, which leads to enhanced π-π packing as demonstrated by the stronger (010) peak of PTP8. The scattering spectra of PTP8:$PC_{71}BM$ blend films with different fullerene ratios are also shown in Figure 3b-f, with the one dimension spectrum shown in Figure 4b. A halo around 1.4 Å^{-1} can be observed in the scattering spectra of all the blend films, which corresponds to a pure amorphous $PC_{71}BM$ phase as formed in the pristine $PC_{71}BM$ film (Figure S10b). The halo in the 1:0.3 film is less prominent, suggesting discontinues pure fullerene phase. This observation is in accordance with the relatively low efficiency and poor electron mobility of the 1:0.3 film. At higher fullerene concentration, the halo is more apparent, indicating increased pure fullerene domains and enhanced electron transport. The diffraction of PTP8:fullerene is evidently stronger than PT8:fullerene (Figure S10c), indicating higher domain crystallinity for both blending components. This observation is also confirmed by the increased selected area diffraction of PTP8 over PT8 and P8 in Figure S11. By GIWAXS investigation, we concluded that the polymer packing orientation is not significantly changed by the side-chain modification. However, reduced π–π stacking distance of PTP8 results in enhanced polymer packing and increased fullerene crystallinity. The high demixing of PTP8 and fullerene at both microscopic and mesoscopic level promotes the forming of continues electron pathways at relatively low fullerene ratio. Yet due to the complexity of blend system and limit of our characterization, other mechanisms cannot be totally ruled out.

It is worth noting that we observed a very unique morphology in the blend film of PTP8 during the investigation. As shown in Figure S12, "valley-like" domains with different sizes are observed in AFM topography and SEM images, which increase in size with increased DIO and fullerene concentration (Figure S13). The bulk morphology of the film was also investigated by high-resolution HAADF-STEM. The valley-like structures were confirmed to be highly crystalline PCBM-rich clusters, which were revealed by the high-intensity diffraction spots[21a] in the GIWAXS spectra of PTP8:fullerene films with a blend ratio of 1:0.8 and 1:1 (Figure 4). To the best of our knowledge, this is the first report of such a highly ordered fullerene structure in a D-A polymer:fullerene blend film. Clearly, the PTP8 seems to induce PCBM crystallization even at low fullerene loading. The alkylphenyl side-chain introduced to the TPD monomer in PTP8 evidently prevents the fullerene intercalation and increases the polymer ordering, which may further help driving the fullerene molecules out of

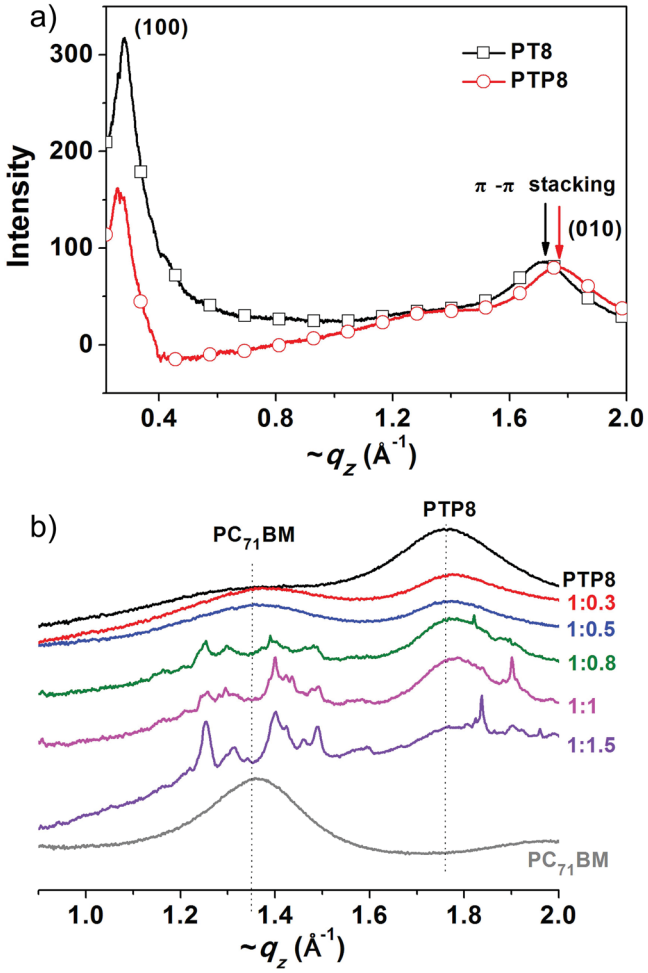

Figure 4. Out-of-plane line cuts from the 2D GIWAXS of PT8 and PTP8 (a) as well as PTP8:$PC_{71}BM$ with different blend ratios (b). Please note that the scattering vectors are approximate as the 2D data have not been corrected for the "missing wedge" of data along the out-of-plane direction.[19]

the polymer matrix and forming pure fullerene phases. However, the enhanced demixing in the PTP8:fullerene film may reduce the fullerene concentration in the mixed regions to below the percolation limit, leading to increased bimolecular recombination [8f] and lower FF than P8 and PT8 (Table S4). At a higher fullerene loading of 1:1.5, the diffraction rings become more sharply defined, which are similar to the diffraction pattern of pure fullerene powders.[21b] Meanwhile, the crystallinity of the polymer-rich domains is decreased with excessive PCBM loading, as confirmed by the reduced intensity of the polymer (010) and (100) peak (Figure S14). We further estimated the sizes of PTP8 crystals with different D/A ratios by using the Debye–Scherrer's equation (Supporting Information). The results indicate that the polymer ordering reaches the highest value around the optimal blend ratio and decreases with higher PCBM loading.

By adopting alkyl aromatic side-chains to both D/A comonomers on the BDT-TPD backbone, a new D-A polymer PTP8 with enhanced thermal stability and packing order was synthesized and demonstrated a high V_{oc} (~1.0 V) and PCE (~6.0%) at a very low blend ratio of 1:0.5. The increased side-chain rigidity and bulkiness prevent the intercalation of fullerenes at a molecular level. The enhanced packing and reduced π-π stacking distance further promote the polymer:fullerene demixing, leading to a large D/A ratio and highly ordered fullerene clusters, which have been observed for the first time in amorphous polymer/fullerene blend films. In general, this "double aromatic side-chains" structure may become a universal design approach for existing polymers to achieve high performance at low fullerene and additive concentration.

Experimental Section

Characterization: UV-vis-NIR spectra were recorded on a Perkin Elmer model Lambda 750. Thermo gravimetric analysis (TGA) was carried out using a Perkin Elmer TGA4000. Tapping-mode AFM images were obtained with a Veeco Multimode V instrument, SEM images were carried out by FEI Scanning Electron Microscope, and EF-TEM & HAADF-STEM were performed on Tecnai G2 F20 S-Twin Transmission Electron Microscope. 2D GIWAXS experiments were conducted at Shanghai Synchrotron Radiation Facility (SSRF) on diffraction beam line (BL14B1).

Synthesis of Polymers: P8 was prepared according to a previous report,[8d] PT8,[9f] and PTF8[22] were synthesized using our previously reported procedure. PTP8 was synthesized according to the procedures as follows: in a 50 mL reaction tube, 2,6-Bis(trimethyltin)-4,8-bis(5-(2-ethylhexyl)thiophen-2-yl)benzo[1,2-b:4,5b']dithiophene (0.22 g, 0.24 mmol), 1,3-dibromo-5-(4-octylphenyl)-5H-thieno[3,4-c]pyrrole-4,6-dione (0.12 g, 0.24 mmol) tri(*o*-tolyl)phosphine (0.02 g, 0.08 mmol), and $Pd_2(dba)_3$ (0.01 g, 0.01 mmol) were dissolved in 5 mL dry toluene under argon. After stirred at 110 °C for 48 h, the mixture was cooled to room temperatures and precipitated in methanol (80 mL). The precipitate was filtered and washed with methanol (24 h) and hexane (24 h) successively in a soxhlet apparatus to remove oligomers and catalyst residue. Finally, the polymer was extracted with chloroform (24 h). The chloroform fraction was concentrated and precipitated in methanol. The precipitate was filtered and dried in vacuum at 80 °C overnight. PTP8 was obtained as dark purple solid (231 mg, 85%), GPC: M_w = 26.1 kg mol^{-1}, PDI = 2.08. The values were determined by using gel permeation chromatography (GPC) at 150 °C in 1,2,4-trichlorobenzene against polystyrene standards, and the molecular structure was supported by ^{1}H NMR spectra (Figure S1). ^{1}H NMR (400 MHz, $CDCl_3$): δ (ppm) 9.00–8.00 (br, 2H ArH), 7.50–6.00 (br, 6H ArH), 3.20–2.20 (br, 6H), 2.00–0.40 (br, H); Elemental analysis calcd (%) for $C_{54}H_{61}NO_2S_5$: C 71.06; H, 7.14; N, 1.48; found: C 70.96, H 7.13, N: 1.47.*Device Fabrication and Testing*: Polymer solar cells were fabricated with a general structure of ITO/PEDOT-PSS (40 nm)/polymer:PCBM /LiF/Al. Patterned ITO glass substrates were cleaned by sequential ultrasonic treatment in detergent, acetone, deionized water and isopropyl alcohol. The organic residue was further removed by treating with UV-ozone for 10 min. A thin film of PEDOT: PSS (~40 nm) was spin-coated on ITO substrates and dried at 150 °C for 10 min. A blend of polymers and PCBM with different ratios was dissolved in chloroform or chlorobenzene containing 0–3% (v/v) diiodooctane, filtered through a 0.45 μm poly(tetrafluoroethylene) (PTFE) filter, spin-coated at 1200 rpm for 40 s, 0.6 nm of LiF (0.2A/s) and 100 nm Al (2A/s) layers were then thermally evaporated on the active layer at a pressure of 1.0×10^{-6} mbar through a shadow mask (active area 7.25 mm^2). The current density–voltage characteristics of the photovoltaic cells were measured using a Keithely 2400 (*I–V*) digital source meter under a simulated AM 1.5G solar irradiation at 100 mW/cm^2 (Newport, Class AAA solar simulator, 94023A-U). The light intensity is calibrated by a certified Oriel Reference Cell (91150V) and verified with a NREL calibrated Hamamatsu S1787–04 diode. The external quantum efficiency (EQE) was performed using a certified IPCE equipment (Zolix Instruments, Inc, SolarCellScan100).

Supporting Information

Supporting Information is available from the Wiley Online Library or from the author.

Acknowledgements

We acknowledge technical support from workers at Shanghai Synchrotron Radiation Facility (SSRF) on diffraction beamline (BL14B1). This work was supported by the National High Technology Research and Development Program of China (863 Program) (Grant No. 2011AA050520), the National Natural Science Foundation of China (Grant No. 61176054), the Natural Science Foundation of Jiangsu Province, China (Grant No. BK2011279), and the Doctoral Fund of Ministry of Education of China (Grant No. 20113201120019).

Received: November 11, 2013
Revised: December 19, 2013
Published online: March 14, 2014

[1] a) G. Yu, J. Gao, J. C. Hummelen, F. Wudl, A. J. Heeger, *Science* **1995**, *270*, 1789; b) Y.-J. Cheng, S.-H. Yang, C.-S. Hsu, *Chem. Rev.* **2009**, *109*, 5868; c) T. D. Nielsen, C. Cruickshank, S. Foged, J. Thorsen, F. C. Krebs, *Sol. Energy Mater. Sol. Cells* **2010**, *94*, 1553; d) H. Zhou, L. Yang, W. You, *Macromolecules* **2012**, *45*, 607; e) Y. F. Li, *Acc. Chem. Res.* **2012**, *45*, 723.

[2] a) C. M. Amb, S. Chen, K. R. Graham, J. Subbiah, C. E. Small, F. So, J. R. Reynolds, *J. Am. Chem. Soc.* **2011**, *133*, 10062; b) S. C. Price, A. C. Stuart, L. Yang, H. Zhou, W. You, *J. Am. Chem. Soc.* **2011**, *133*, 4625; c) T.-Y. Chu, J. Lu, S. Beaupré, Y. Zhang, J.-R. m. Pouliot, S. Wakim, J. Zhou, M. Leclerc, Z. Li, J. Ding, Y. Tao, *J. Am. Chem. Soc.* **2011**, *133*, 4250; e) Y. Huang, X. Guo, F. Liu, L. Huo, Y. Chen, T. P. Russell, C. C. Han, Y. Li, J. Hou, *Adv. Mater.* **2012**, *23*, 4636.

[3] a) L. Dou, J. You, J. Yang, C.-C. Chen, Y. He, S. Murase, T. Moriarty, K. Emery, G. Li, Y. Yang, *Nat. Photonics* **2012**, *6*, 180; b) J. You, L. Dou, K. Yoshimura, T. Kato, K. Ohya, T. Moriarty, K. Emery, C.-C. Chen, J. Gao, G. Li, Y. Yang, *Nat. Commun.* **2013**, *4*, 1446.

[4] a) S. H. Park, A. Roy, S. Beaupré, S. Cho, N. Coates, J. S. Moon, D. Moses, M. Leclerc, K. Lee, A. J. Heeger, *Nat. Photonics* **2009**, *3*, 297; b) L. Dou, J. Gao, E. Richard, J. You, C.-C. Chen, K. C. Cha, Y. He, G. Li, Y. Yang, *J. Am. Chem. Soc.* **2012**,*134*,10071; c) Z. He, C. Zhong, S. Su, M. Xu, H. Wu, Y. Cao, *Nat. Photonics* **2012**, *6*, 591; d) Y.-X. Xu, C.-C. Chueh, H.-L. Yip, F.-Z. Ding, Y.-X. Li, C.-Z. Li, X. Li, W.-C. Chen, A. K. Y. Jen, *Adv. Mater.* **2012**, *24*, 6356.

[5] a) J. M. Warman, M. P. de Haas, T. D. Anthopoulos, D. M. de Leeuw, *Adv. Mater.* **2006**, *18*, 2294; b) W. Y. Huang, P. T. Huang, Y. K. Han, C. C. Lee, T. L. Hsieh, M. Y. Chang, *Macromolecules* **2008**, *41*, 7485; c) T. Agostinelli, S. Lilliu, J. G. Labram, M. C.-Quiles, M. Hampton, E. Pires, J. Rawle, O. Bikondoa, D. D. C. Bradley, T. D. Anthopoulos, J. Nelson, J. E. Macdonald, *Adv. Funt. Mater.* **2011**, *21*, 1701.

[6] A. C. Mayer, M. F. Toney, S. R. Scully, J. Rivnay, C. J. Brabec, M. Scharber, M. Koppe, M. Heeney, I. McCulloch, M. D. McGehee, *Adv. Funct. Mater.* **2009**, *19*, 1173.

[7] N. C. Miller, E. Cho, M. J. N. Junk, R. Gysel, C. Risko, D. Kim, S. Sweetnam, C. E. Miller, L. J. Richter, R. J. Kline, M. Heeney, I. McCulloch, A. Amassian, D. Acevedo-Feliz, C. Knox, M. R. Hansen, D. Dudenko, B. F. Chmelka, M. F. Toney, J.-L. Brédas, M. D. McGehee, *Adv. Mater.* **2012**, *24*, 6071.

[8] a) Y. Zhang, S. K. Hau, H.-L. Yip, Y. Sun, O. Acton, A. K.-Y. Jen, *Chem. Mater.* **2010**, *22*, 2696; b) G. Zhang, Y. Fu, Q. Zhang, Z. Xie, *Chem. Commun.* **2010**, *46*, 4997; c) Y. Zou, A. Najari, P. Berrouard, S. Beaupré, B. B. Réda Aïch, Y. Tao, M. Leclerc, *J. Am. Chem. Soc.* **2010**, *132*, 5330; d) C. Piliego, T. W. Holcombe, J. D. Douglas, C. H. Woo, P. M. Beaujuge, J. M. J. Fréchet, *J. Am. Chem. Soc.* **2010**, *132*, 7595; e) E. T. Hoke, K. Vandewal, J. A. Bartelt, W. R. Mateker, J. D. Douglas, R. Noriega, K. R. Graham, J. M. J. Fréchet, A. Salleo, M. D. McGehee, *Adv. Energy Mater.* **2012**, *3*, 220; f) J. A. Bartelt, Z. M. Beiley, E. T. Hoke, W. R. Mateker, J. D. Douglas, B. A. Collins, J. R. Tumbleston, K. R. Graham, A. Amassian, H. Ade, J. M. J. Fréchet, M. F. Toney, M. D. McGehee, *Adv. Energy Mater.* **2012**, *3*, 364.

[9] a) L. Huo, J. Hou, S. Zhang, H.-Y. Chen, Y. Yang, *Angew. Chem. Int. Ed.* **2010**, *49*, 1500; b) L. J. Huo, S. Q. Zhang, X. Guo, F. Xu, Y. F. Li, J. H. Hou, *Angew. Chem., Int. Ed.* **2011**, *50*, 9697; c) R. Duan, L. Ye, X. Guo, Y. Huang, P. Wang, S. Zhang, J. Zhang, L. Huo, J. Hou, *Macromolecules* **2012**, *45*, 3032; d) M. Wang, X. Hu, P. Liu, W. Li, X. Gong, F. Huang, Y. Cao, *J. Am. Chem. Soc.* **2011**, *133*, 9638; e) J. Yuan, X. Huang, F. Zhang, J. Lu, Z. Zhai, C. Di, Z. Jiang, W. Ma, *J. Mater. Chem.* **2012**, *22*, 22734; f) J. Yuan, Z. Zhai, H. Dong, J. Li, Z. Jiang, Y. Li, W. Ma, *Adv. Funct. Mater.* **2013**, *23*, 885.

[10] D. Qian, W. Ma, Z. Li, X. Guo, S. Zhang, L. Ye, H. Ade, Z. Tan, J. Hou, *J. Am. Chem. Soc.* **2013**, *135*, 8464.

[11] B.-G. Kim, X. Ma, C. Chen, Y. Ie, E. W. Coir, H. Hashemi, Y. Aso, P. F. Green, J. Kieffer, J. Kim, *Adv. Funct. Mater.* **2013**, *23*, 439.

[12] a) J. K. Lee, W. L. Ma, C. J. Brabec, J. S. Moon, J. Y. Kim, K. Lee, G. C. Bazan, A. J. Heeger, *J. Am. Chem. Soc.* **2008**, *130*, 3619; b) S. J. Lou, J. M. Szarko, T. Xu, L. Yu, T. J. Marks, L. X. Chen, *J. Am. Chem. Soc.* **2011**, *133*, 20661; c) X. Guo, C. Cui, M. Zhang, L. Huo, Y. Huang, J. Hou, Y. Li, *Energy Environ. Sci.* **2012**, *5*, 7943; d) Y. Gu, C. Wang, T. P. Russell, *Adv. Energy Mater.* **2012**, *2*, 683.

[13] Y. Sun, G. C. Welch, W. L. Leong, C. J. Takacs, G. C. Bazan, A. J. Heeger, *Nat. Mater.* **2012**, *11*, 44.

[14] W. Ma, C. Yang, X. Gong, K. Lee, A. J. Heeger, *Adv. Funct. Mater.* **2005**, *15*, 1617.

[15] a) C. Melzer, E. J. Koop, V. D. Mihailetchi, P. W. M. Blom, *Adv. Funct. Mater.* **2004**, *14*. 865; b) V. D. Mihailetchi, L. J. A. Koster, P. W. M. Blom, C. Melzer, B. de Boer, J. K. J. van Duren, R. A. J. Janssen, *Adv. Funct. Mater.* **2005**, *15*, 795; c) S. M. Tuladhar, D. Poplavskyy, S. A. Choulis, J. R. Durrant, D. D. C. Bradley, J. Nelson, *Adv. Funct. Mater.* **2005**, *15*, 1171.

[16] W. Ma, L. Ye, S. Zhang, J. Hou, H. Ade, *J. Mater. Chem. C* **2013**, *1*, 5023.

[17] a) N. D. Treat, M. A. Brady, G. Smith, M. F. Toney, E. J. Kramer, C. J. Hawker, M. L. Chabinyc, *Adv. Energy Mater.* **2011**, *1*, 82; b) N. D. Treat, A. V. Christopher, J. Takacs, N. Batara, M. Al-Hashimi, M. J. Heeney, A. J. Heeger, F. Wudl, C. J. Hawker, M. L. Chabinyc, *J. Am. Chem. Soc.* **2012**, *134*, 15869; c) B. A. Collins, E. Gann, L. Guignard, X. He, C. R. McNeill, H. Ade, *J. Phys. Chem. Lett.* **2010**, *1*, 3160; d) B. A. Collins, J. R. Tumbleston, H. Ade, *J. Phys. Chem. Lett.* **2011**, *2*, 3135; e) B. A. Collins, Z. Li, J. R. Tumbleston, E. Gann, C. R. McNeill, H. Ade, *Adv. Energy Mater.* **2013**, *3*, 65; f) W. Yin, M. Dadmunet, *ACS Nano* **2011**, *5*, 4756; g) D. R. Kozub, K. Vakhshouri, L. M. Orme, C. Wang, A. Hexemer, E. D. Gomez, *Macromolecules* **2011**, *44*, 5722; h) Y. Sun, S. C. Chien, H. L. Yip, K. S. Chen, Y. Zhang, J. A. Davies, F. C. Chen, B. Lin, A. K.-Y. Jen, *J. Mater. Chem.* **2012**, *22*, 5587.

[18] a) C. J. Brabec, M. Heeney, I. McCulloch, J. Nelson, *Chem. Soc. Rev.* **2011**, *40*, 1185; b) J. E. Slota, X. He, W. T. S. Huck, *Nano Today* **2010**, *5*, 231; c) J. S. Kim, Y. Lee, J. H. Lee, J. H. Park, J. K. Kim, K. Cho, *Adv. Mater.* **2010**, *22*, 1355.

[19] J. Rivnay, S. C. Mannsfeld, C. E. Miller, A. Salleo, M. F. Toney, *Chem. Rev.* **2012**, *112*, 5488.

[20] J. D. Yuen, F. Wudl, *Energy Environ. Sci.* **2013**, *6*, 392.

[21] a) E. Verploegen, R. Mondal, C. J. Bettinger, S. Sok, M. F. Toney, Z. Bao, *Adv. Funct. Mater.* **2010**, *20*, 3519; b) M. Casalegno, S. Zanardi, F. Frigerio, R. Po, C. Carbonera, G. Marra, T. Nicolini, G. Raos, S. V. Meille, *Chem. Commun.* **2013**, *49*, 4525.

[22] J. Yuan, Y. Zang, H. Dong, G. Liu, C. Di, Y. Li, W. Ma, *Poly. Chem.* **2013**, *4*, 4199.